Self-focusing non-diffracting special beam in hyperbolic media

Yueqian Zhang, Haotian Wu, Chongwu Wang, Guanghui Yuan, Linyang Zou, Qian Wang, Qi Jie Wang*, and Yu Luo**

Yueqian Zhang, Haotian Wu, Chongwu Wang, Linyang Zou, Qi Jie Wang
School of Electrical and Electronic Engineering, Nanyang Technological University, Singapore 639798, Singapore
E-mail: qjwang@ntu.edu.sg

Yueqian Zhang, Qian Wang
Institute of Materials Research and Engineering, Agency for Science, Technology and Research (A*STAR), 2 Fusionopolis Way, Innovis, Singapore, 138634, Singapore
E-mail: wangqian@imre.a-star.edu.sg

Guanghui Yuan
Department of Optics and Optical Engineering, School of Physical Sciences, University of Science and Technology of China, Hefei 230026, China

Yu Luo
National Key Laboratory of Microwave Photonics, Nanjing University of Aeronautics and Astronautics, Nanjing, China
E-mail: yu.luo@nuaa.edu.cn

Keywords: special beam, hyperbolic media, self-focusing effect

Abstract:

The field of non-diffracting special beams, distinguished by their non-diffracting characteristics during propagation in free space, has experienced substantial progress over the last decade. However, the exploration of special beams has been predominantly focused on isotropic background media, with limited attention given to their behavior in anisotropic backgrounds, such as elliptical or hyperbolic media. In this study, we investigate the characteristics of non-diffracting wave propagation in anisotropic media, specifically the hyperbolic media by means of using α-MoO_3, a van der Waals (vdW) crystal that supports in-plane hyperbolic surface phonon polaritons in the mid-infrared spectrum as the platform. Specifically, we demonstrate that the special beams can be constructed under various isofrequency contours by the application of coordinate transformation scheme. More intriguingly, we reveal that the special beam propagation in hyperbolic medium can exhibit the distinctive feature of self-focusing. Our investigation provides new perspectives for the understanding of special beam formations and introduces new possibilities for complex beam manipulation in extreme anisotropic environments within the mid-infrared (MIR) regime.

1. Introduction

Non-diffracting beams are a family of special waveforms characterized by the non-diffracting envelope during propagation in free space. The first found non-diffracting beam is the Airy beam, which arises from a unique solution of the Schrödinger equation and was further extended to optical regime in 2007[1]. The most striking feature of the Airy beam is that the beam shape is maintained during wave propagation. Meanwhile, the main lobe trajectory of the Airy beam follows a parabola in the paraxial range. Subsequently, researchers have endeavored to extend the concept of non-diffracting beams into the non-paraxial regimes with varying main lobe trajectories, leading to the proposal of various non-diffracting beams. For instance, the trajectory of the half Bessel beam follows a circular path[2], the trajectory of the Weber beam follows a parabolic path[3], and the trajectory of the Mathieu beam aligns with an ellipse. These special beams exhibit non-diffracting characteristics beyond the paraxial range, enabling their trajectories to achieve bending angles approaching nearly 90 degrees. In addition, a variety of other special beams have also been reported, including abruptly autofocusing beams[4], arbitrary

trajectory beams[5], Cosine-Gauss beams[6], and more recently, Airy-like shear polaritons in hyperbolic media[7].

However, the majority of these special beams have been studied primarily in isotropic media such as free space. Only in recent years have researchers begun to explore how special beams form and propagate in anisotropic environments. A notable example is the recent demonstration of an Airy-like surface polariton in a hyperbolic van der Waals crystal[7].

Despite these advances, a general and unified design principle capable of constructing special beams across all classes of media—including isotropic, elliptic anisotropic, and hyperbolic media—has yet to be systematically established.

To address this gap, we present a general design principle applicable to all kinds of media. Specifically, by employing the proposed scheme in hyperbolic media, a special beam that exhibits the unique property of self-focusing can be realized.

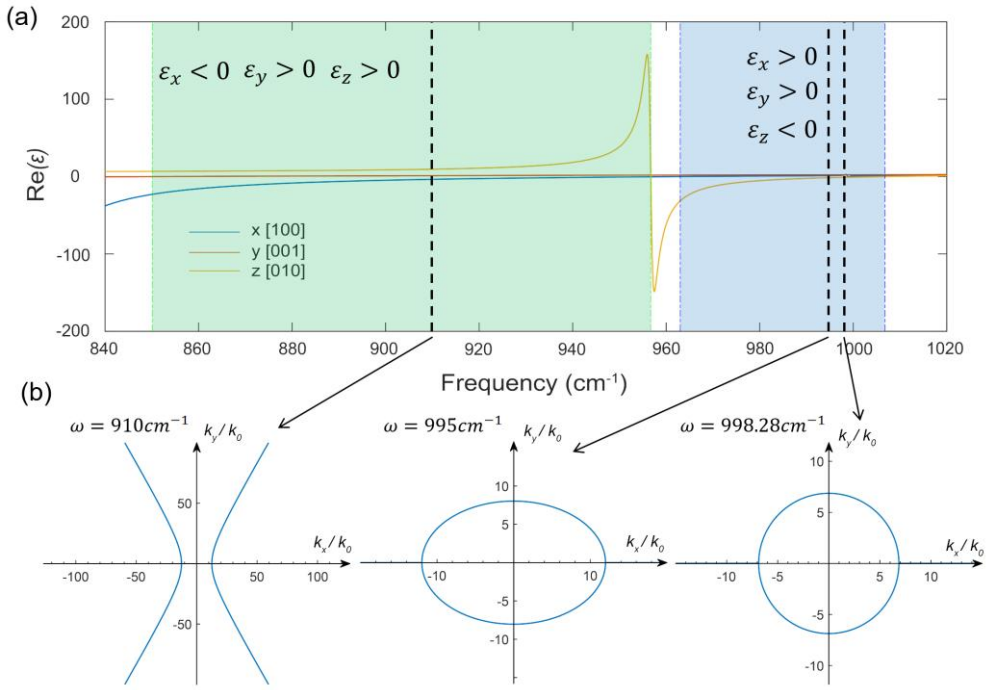


Figure 1. (a) The real part of the permittivity along x, y and z directions of α-MoO_3. The green highlighted region supports in-plane hyperbolic surface phonon polariton and the blue highlighted region supports elliptical or circular surface wave. (b) The isofrequency contour of surface phonon polariton at different frequencies. At 910cm^{-1}, the contour is hyperbola, at 995cm^{-1} it becomes an ellipse, while at 998.28cm^{-1}, it's a circle like free space.

2. Isofrequency coutour of α-MoO_3

A prevalent approach to generating special beams involves the utilization of two-dimensional (2D) surface plasmon polariton (SPP) platforms, with various design strategies proposed to achieve this objective. The pioneering work in this field was reported in 2010 by Salandrino and Christodoulides, who has introduced the concept of 'Airy plasmons' and theoretically demonstrated that a self-healing and self-accelerating Airy beam could be realized on an SPP platform through precise manipulation of the transverse field profile[8].

Building upon this foundation, numerous implementations have been developed. One straightforward method involves directly coupling a free-space Airy beam onto the surface wave platform through a periodic grating structure, as demonstrated by Zhang et al.[9]. Alternatively, metasurface-assisted generation of surface waves has been extensively explored. The fundamental principle is to impart the unique phase distribution characteristic of special beams onto the surface wave platform. For instance, Minovich et al. introduced a coupling phase grating on a gold thin-film SPP platform to imprint the initial phase distribution of an Airy beam[10]. This phase grating technique has since been widely adopted to generate and control various special beams[6,11–13], enabling applications such as controlling the spatial position of plasmonic hot spots for subwavelength field shaping[11], providing dynamic insights into propagating special beam pulses[13], and generating Cosine-Gauss beams[6]. Other methodologies encompass binary phase mask[5], in-plane diffraction patterning[14,15], Fourier transformation gratings[16], mode-matching metasurfaces[17], Pancharatnam–Berry (PB) phase metasurfaces[18] and so on.

The implementation of surface wave special beams has also been extended to 2D materials. Realization of Airy beams on graphene plasmon platforms have been proposed[19], with demonstrations in the terahertz regime[20]. More recently, Bai et al. demonstrated hyperbolic shear polariton beams with Airy-like profiles in van der Waals crystals[7]. High order optical angular momentum (OAM) beam was used to excite the circular disk antenna on the van der Waals crystals to generate the Airy-like beam.

To demonstrate our design principle, we aim to find a platform capable of flexibly exciting isofrequency contours, particularly hyperbolic isofrequency contours. Traditional hyperbolic media can be realized with metamaterial or metasurface. With effective medium theory, periodically arranged deep subwavelength unit cell can be regarded as an effective homogenous media with new permittivity and permeability. Based on this theory, numerous hyperbolic metamaterial and metasurface designs have been proposed, including metal/dielectric multi-

layer[21,22], metal nanowire array[23], metal nano grating[24] and anisotropic conductive layer[25]. However, all these metamaterial/metasurface based hyperbolic media typically require complicated fabrication processes and are unsuitable for high-frequency applications due to finite size limitations. The emergence of van de Waals crystals in recent years provides a potential solution to our approach. Van de Waals crystal typically consists of layered structures and is bonded by the van de Waals force between layers. They exhibit strong phonon resonance in the mid-infrared (MIR) regime and surface wave is supported, much like the surface plasmon system used to demonstrate the traditional special beams.

Among the various van der Waals materials, α-MoO_3 stands out due to its unique ability to support in-plane hyperbolic surface waves[26–28], making it an ideal platform for demonstrating our specialized beam design. α-MoO_3 is a layered two-dimensional material that exhibits strong phonon resonances in the mid-infrared (MIR) regime, enabling the propagation of highly confined surface phonon polaritons. Notably, the isofrequency contours of these surface waves undergo a frequency-dependent evolution—from nearly isotropic circular shapes to anisotropic ellipses, and ultimately to highly anisotropic open hyperbola. This distinctive hyperbolic dispersion has inspired a broad range of studies. For instance, twisted moiré heterostructures based on α-MoO_3 have been proposed and investigated, revealing topological transitions in polariton dispersion and enabling complex light matter interactions governed by the underlying hyperbolic isofrequency contours[29–33]. In parallel, significant progress has been made in understanding and engineering hybridized polariton systems[34–38], where phonon polaritons couple with other quasiparticles, as well as in developing mechanisms for tuning phonon polariton propagation via chemical doping or structure shaping[39–42]. Furthermore, a variety of strategies have been demonstrated for manipulating surface polariton waves on α-MoO_3 such as geometric structuring or gate tuning.[43–46], further showcasing the versatility of this platform for advanced polaritonic beam engineering and photonic applications[47,48].

To design the special beam, we must know the exact parameters of the isofrequency contour.. The permittivity of α-MoO_3 can be modeled as a Coupled Lorentz model[49]:

$$\varepsilon_x(\omega) = \varepsilon_x^{\infty}\left[\frac{(\omega_{x1}^{LO})^2-\omega^2-i\gamma_{x1}\omega}{(\omega_{x1}^{TO})^2-\omega^2-i\gamma_{x1}\omega}\right]\left[\frac{(\omega_{x2}^{LO})^2-\omega^2-i\gamma_{x2}\omega}{(\omega_{x2}^{TO})^2-\omega^2-i\gamma_{x2}\omega}\right]\left[\frac{(\omega_{x3}^{LO})^2-\omega^2-i\gamma_{x3}\omega}{(\omega_{x3}^{TO})^2-\omega^2-i\gamma_{x3}\omega}\right]$$

$$\varepsilon_y(\omega) = \varepsilon_y^{\infty}\left[\frac{(\omega_{y1}^{LO})^2-\omega^2-i\gamma_{y1}\omega}{(\omega_{y1}^{TO})^2-\omega^2-i\gamma_{y1}\omega}\right] \quad (1)$$

$$\varepsilon_z(\omega) = \varepsilon_z^{\infty}\left[\frac{(\omega_{z1}^{LO})^2 - \omega^2 - i\gamma_{z1}\omega}{(\omega_{z1}^{TO})^2 - \omega^2 - i\gamma_{z1}\omega}\right]$$

By incorporating the phonon frequency and damping factor parameters from the previous study[49], the permittivity of α-MoO_3 can be determined. As shown in Figure 1a, from 850 cm^{-1} to 956 cm^{-1}, α-MoO_3 has the unique in-plane hyperbolic permittivity, where ε_x [100] direction is negative while ε_y [001] direction is positive and ε_z [010] is positive. Therefore, the surface phonon polariton in this region has the hyperbolic isofrequency contour. And from 963 cm^{-1} to 1007 cm^{-1}, out-of-plane hyperbolic permittivity is achieved ($\varepsilon_x > 0, \varepsilon_y > 0, \varepsilon_z < 0$) and the isofrequency contour of the in-plane surface phonon polariton can be a circle or an ellipse depending on the excitation frequency. In these two regions, α-MoO_3 serves as a perfect platform to demonstrate our special beam design principle as we can choose different frequency to have different contours. Here we consider a layer of α-MoO_3 with a thickness of 300 nm deposited onto a silicon substrate. By utilizing the equation that describes surface waves in a biaxial slab embedded between two semi-infinite media, we can analytically calculate the propagation constant of the surface wave[50]:

$$\beta = \frac{\rho}{d}\left[\arctan\left(\frac{\varepsilon_1\rho}{\varepsilon_z}\right) + \arctan\left(\frac{\varepsilon_3\rho}{\varepsilon_z}\right) + \pi l\right], l = 0,1,2 \ldots \quad (2)$$

Where d is the thickness of α-MoO3, ε_1 and ε_3 are the permittivity of superstrate and substrate, $\rho = i\sqrt{\frac{\varepsilon_z}{\varepsilon_x\cos^2\alpha + \varepsilon_y\sin^2\alpha}}$.

Using this equation, we can calculate the isofrequency contour at a given frequency. For in-plane hyperbolic region, we choose $\omega = 910cm^{-1}$, $\varepsilon_1 = 1$ for the air and $\varepsilon_3 = 13$ for the Si substrate. For α-MoO_3 at this frequency, the dielectric constants are $\varepsilon_x = -3.56, \varepsilon_y = 1.21, \varepsilon_z = 9.52$. Taking these parameters into the equation (2) and the isofrequency contour can be obtained as illustrated by Figure 1b. The resulting dispersion relation can be characterized by a hyperbola as:

$$\frac{k_x^2}{\varepsilon_{effy}} + \frac{k_y^2}{\varepsilon_{effx}} = k_0^2 \quad (3)$$

Where $\varepsilon_{effy} = [\frac{\mathrm{Re}(\beta_x)}{k_0}]^2 = 158.1$ and $\varepsilon_{effx} = \varepsilon_{effy}\frac{\varepsilon_x}{\varepsilon_y} = -467.5$. And β_x is the propagating constant along x direction when $\alpha = 0$.

This configuration indicates that ε_{effy} is positive while ε_{effx} is negative, demonstrating that the in-plane surface phonon polariton serves as a perfect natural hyperbolic media.

For the out-of-plane hyperbolic region, when $\omega = 998.28cm^{-1}$, the permittivity components will be $\varepsilon_x = \varepsilon_y = 2.37,$ and $\varepsilon_z = -0.95$. Substituting these values into equation (2) and we can obtain the effective permittivity components: $\varepsilon_{eff} = \varepsilon_{effx} = \varepsilon_{effy} \approx 47$. Consequently, the isofrequency contour of surface wave is a circle, analogous to that in free space.

When it comes to $\omega = 995cm^{-1}$, the permittivity of α-MoO3 changes to: $\varepsilon_x = 1.25, \varepsilon_y = 2.34, \varepsilon_z = -1.42$. Accordingly, the resulting in-plane isofrequency contour becomes an ellipse with the effective permittivities of $\varepsilon_{effx} = 64.51, \varepsilon_{effy} = 143.73$.

By utilizing these three specific frequency points, we will demonstrate how to construct special beams based on a unified design principle applied across different media, ranging from isotropic circle to anisotropic ellipse and finally extreme anisotropic hyperbola.

3. Special beam design in different media

Given the diversity of isofrequency contours, it is natural to consider transforming the special beams from isotropic media into ellipse and hyperbolic media. Suppose there is a beam in isotropic media with permittivity ε starting from $x = 0$ and propagating towards positive x direction. The beam can be regarded as the superposition of multiple plane waves propagating towards different angles. In this case, the components of the wavevector are given by $k_x = \sqrt{\varepsilon}k_0\cos\theta, k_y = \sqrt{\varepsilon}k_0\sin\theta$. Here, θ is the angle between the momentum k and positive x direction, which ranges from $-\frac{\pi}{2}$ to $-\frac{\pi}{2}$. Accordingly, the electrical field can be expressed as:

$$E(x \geq 0, y) = \int_{-\frac{\pi}{2}}^{\frac{\pi}{2}} A(\theta) \exp\left(i\sqrt{\varepsilon}k_0\cos\theta x + i\sqrt{\varepsilon}k_0\sin\theta y\right) d\theta \qquad (4)$$

where $A(\theta)$ is the amplitude and initial phase of each plane wave component. Notably, the beam profile can be modified by adjusting the function $A(\theta)$.When $A(\theta) = \exp(in\theta)$ with $n = 1,2,3\ldots$, this configuration corresponds to the Half Bessel beam[2] whose main lobe can propagate along a circular trajectory and the center position of the circle can also be tuned by shifting the y axis by introducing another constant C to the equation (4) which can lead to the following expression: (detailed explanation can be found in the supporting material) :

$$E(x \geq 0, y) = \int_{-\frac{\pi}{2}}^{\frac{\pi}{2}} A(\theta)\exp(ik_0\cos\theta x + ik_0\sin\theta y)d\theta$$

$$A(\theta) = \exp(in\theta - ik_0 \sin\theta C), n = 1,2,3.. \quad (5)$$

If we construct a beam whose initial electrical field on $x = 0$ plane is:

$$E(x = 0, y) = \int_{-\frac{\pi}{2}}^{\frac{\pi}{2}} \exp(in\theta - ik_0 \sin\theta C)\exp(ik_0 \sin\theta y)d\theta\,, n = 1,2,3\ldots \quad (6)$$

The produced beam will propagate towards positive $\boldsymbol{x}$ direction and the main lobe will follow the circular trajectory as expected. Taking into account the in-plane isofrequency parameter ε_{eff} of α-MoO_3 at $\omega = 998.28cm^{-1}$, we plot the Half Bessel beam in this case. The beam is centered at $y = 0$, indicating no lateral shift, and thus the constant $C = 0$. It can be observed that the main lobe indeed follows a circular trajectory and when it converts to about 90 degree the beam cannot maintain its shape because light cannot propagate backwards as shown in Figure 2(a).

Suppose the medium is no longer isotropic with a circular isofrequency contour but instead exhibits an elliptical isofrequency contour, as α-MoO_3 at $\omega = 995cm^{-1}$. We can still construct the special beam based on the superposition of plane waves, similar to the isotropic case. However, adjustments are necessary due to the change in the isofrequency contour. It's noticed that the weights of each plane wave component can be preserved, which means keeping $A(\theta)$ unchanged and only modify the momentum items to fulfill the new isofrequency contour as well. In the ellipse case, the field profile can be represented as:

$$E(x \geq 0, y) = \int_{-\frac{\pi}{2}}^{\frac{\pi}{2}} A(\theta)\exp[i\sqrt{\varepsilon_y}k_0 \cos\theta x + i\sqrt{\varepsilon_x}k_0 \sin\theta(y)]d\theta$$

$$A(\theta) = \exp(in\theta - ik_0 \sin\theta C), n = 1,2,3\ldots \quad (7)$$

In this case, the wavevector components are given by $k_x = \sqrt{\varepsilon_y}k_0 \cos\theta$ and $k_y = \sqrt{\varepsilon_x}k_0 \sin\theta$, which satisfy the elliptical isofrequency contour equation $\frac{k_x^2}{\varepsilon_y} + \frac{k_y^2}{\varepsilon_x} = k_0^2$. By incorporating the permittivity values of α-MoO_3 at $\omega = 995cm^{-1}$, it can be observed from Figure

2(b) that the main lobe of the special beam becomes an ellipse with the non-diffracting feature is preserved, confirming the effectiveness of the proposed modification.

However, when the isofrequency contour transits from an ellipse to a hyperbola, specifically when ε_x becomes negative, the previous equation cannot be employed. This is because $\sqrt{\varepsilon_x}$ becomes purely imaginary in such case, leading the field intensity at the plane $x = 0$ to diverge. Consequently, the solution is not physically supported. Therefore, to maintain the weights of

each plane wave component $A(\theta)$ unchanged, further adjustment to the momentum items is needed. In this case, we notice that $\sec^2\theta - \tan^2\theta = 1$. So, we can change the k_x and k_y from:

$$k_x = \sqrt{\varepsilon_y}k_0\cos\theta, k_y = \sqrt{\varepsilon_x}k_0\sin\theta \tag{8}$$

To:

$$k_x = \sqrt{\varepsilon_y}k_0\sec\theta, k_y = \sqrt{|\varepsilon_x|}k_0\tan\theta \tag{9}$$

Accordingly, the hyperbolic isofrequency contour is fulfilled by substituting k_x and k_y back into equation:

$$\frac{k_x^2}{\varepsilon_y} + \frac{k_y^2}{\varepsilon_x} = k_0^2(\sec^2\theta - \tan^2\theta) = k_0^2 \tag{10}$$

In this case, the beam is transformed into:

$$E(x \geq 0, y) = \int_{-\frac{\pi}{2}}^{\frac{\pi}{2}} A(\theta)\exp[i\sqrt{\varepsilon_y}k_0\sec\theta x + i\sqrt{|\varepsilon_x|}k_0\tan\theta y]d\theta$$

$$A(\theta) = \exp(in\theta - ik_0\sin\theta C), n = 1,2,3 \ldots \tag{11}$$

By considering α-MoO_3 at the frequency of $\omega = 910cm^{-1}$, we observe that the special beam changes into a brand-new shape, as shown in Figure. 2(c), however, its non-diffracting property is still preserved.

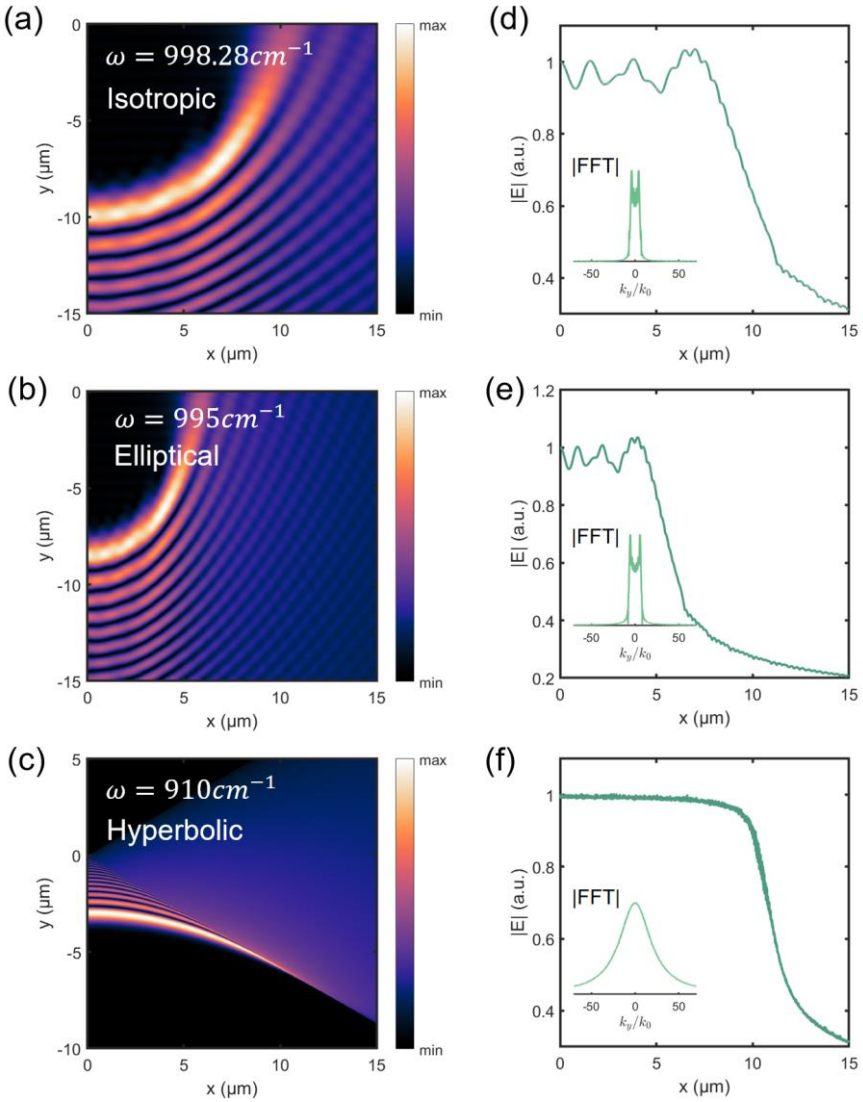


Figure 2. (a-c) The field distribution of special beam in isotropic, elliptical and hyperbolic media. (d-f) The intensity profile of the electrical field of the main lobe. The main lobe of the special beam in hyperbolic media exhibits a longer propagation length. The inset shows the spatial frequency component of each special beam. The special beam in hyperbolic media has a much broader spatial frequency range than the other two beams, resulting in a much smaller aperture requirement.

Based on the above analysis, the design of special can be summarized as follow: we consider the beam system as a superposition of multiple plane waves propagating in different directions, spanning from $-\frac{\pi}{2}$ to $\frac{\pi}{2}$. By utilizing the known weights of each plane wave component required to construct the special beam in isotropic media, we can adapt these components for elliptical and hyperbolic media by modifying the corresponding momentum terms to satisfy the new isofrequency contour. In this way, the non-diffracting property is effectively preserved, enabling the realization of the special beam in these media.

We notice that the change of beam from isotropic media to ellipse contour media is subtle. The only difference is that the trajectory of the main lobe shifts from a circular to an elliptical path. However, when it comes to hyperbolic media, the change is significant. In such case, the main lobe can preserve its energy for a longer propagating length. As shown in Figure 2d, after propagating 10μm along the x direction, the main lobe still maintains nearly 95% of its original intensity, whereas in isotropic and elliptical media, the intensity has decreased substantially.

Another noteworthy point is the significant change in the spatial frequency components of the beam. We conduct Fourier transformation to all these three beams at the beginning $x = 0$ plane and present the results in the inset of Figure 2d-f. From these results, we find that the beam in hyperbolic media exhibits a much broader spatial frequency range, allowing it to be excited with a much smaller aperture. In contrast, the beams in isotropic and elliptical media have a quite limited spatial frequency range, which necessitates a much wider aperture for excitation. Theoretically, a perfect special beam in isotropic and elliptical media requires an infinitely large initial aperture for excitation, as shown in Figure S1a-b. This is because the intensity profile of the beam extends indefinitely in the negative y-direction without a natural cutoff. Consequently, supporting a perfect Half-Bessel beam in such media requires an infinite amount of energy, which is physically unrealizable.

In practical applications, this issue is typically addressed by truncating the input aperture using a Heaviside function or other windowing schemes, resulting in a quasi-special beam, often referred to as a finite-energy special beam, which has been widely adopted in experimental and applied contexts[1,3].

In contrast, the hyperbolic medium does not suffer from this limitation. As shown in Figure S1c, the intensity profile of the beam is inherently localized near the center, indicating that a perfect special beam can be supported within a finite spatial region. This property eliminates the need for infinite aperture and energy, offering a clear practical advantage for beam generation in hyperbolic media.

The distinct behaviors of hyperbolic and elliptical media under the same excitation scheme originate from the topological difference in their isofrequency contours. In hyperbolic media, the corresponding isofrequency contour is an open hyperbola, allowing both k_x and k_y to extend to infinity. In contrast, elliptical media exhibits a closed elliptical contour, constraining both k_x and k_y within finite bounds, as illustrated in Figure 1b. Such fundamental topological difference gives rise to the observed divergence in spatial wave behavior.

One clear manifestation of this difference lies in their spatial spectral characteristics. Due to the unbounded momentum in hyperbolic media, the corresponding real-space distribution can be tightly localized, as permitted by the Fourier uncertainty principle $\Delta k \cdot \Delta x \geq \frac{1}{2}$. In contrast, isotropic and elliptical media, with their limited momentum bandwidth, impose a lower bound on the spatial extent of the beam. As a result, generating a well-formed special beam in isotropic media theoretically requires an infinitely large aperture to encompass the full real-space footprint implied by the limited k-space support.

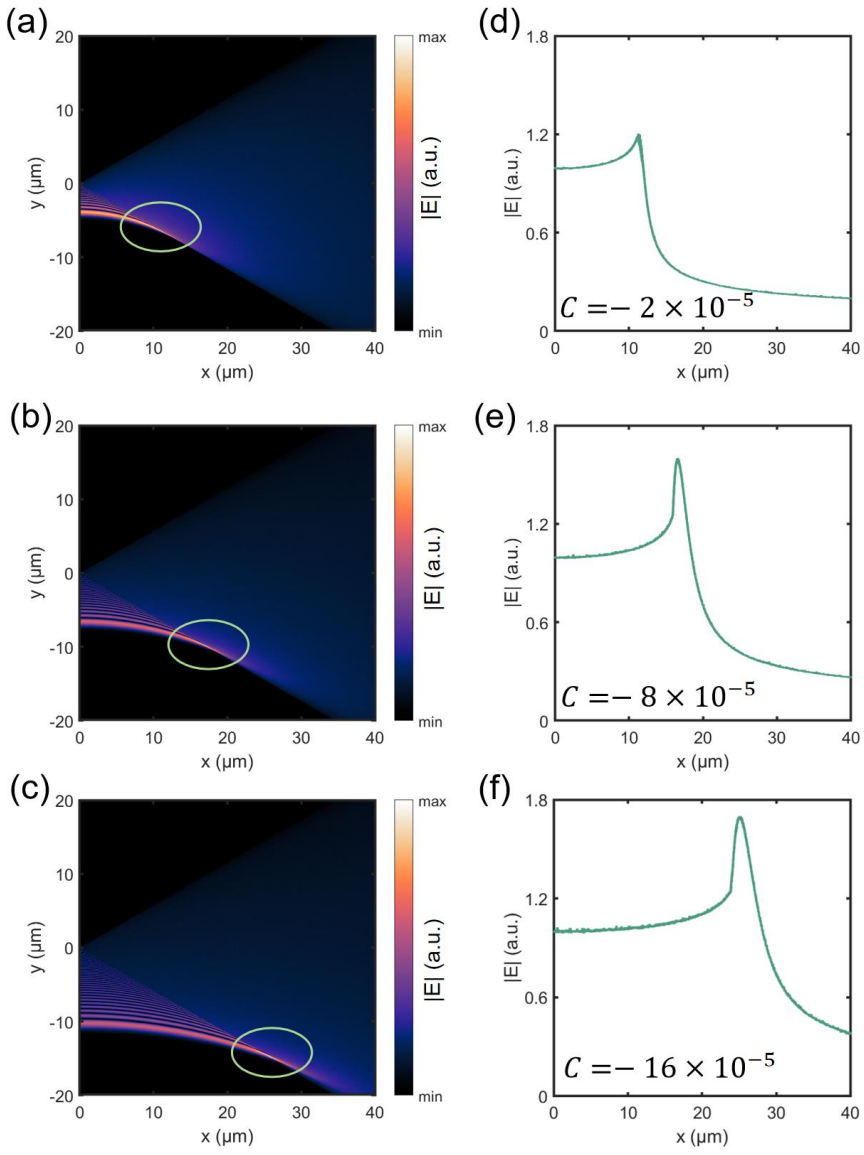


Figure 3. (a-c) The field distribution of special beam in hyperbolic media under different shift values at $\omega = 910cm^{-1}$. With greater shift, the beam is shifted downwards. (d) The normalized electrical field profile along the main lobe. As the absolute value of shift increases from zero, a focusing effect occurs. The greater the shift value, the longer the propagation length and the higher the field enhancement.

4. Self-focusing effect

In addition to exhibiting longer propagation distances and requiring finite apertures, the beam in hyperbolic media possesses the unique property of self-focusing. We notice that when there is no shift ($C = 0$) in the initial field distribution, the special beam in hyperbolic media does not exhibit significant intensity enhancement. However, introducing the shift of the center position C of the initial field distribution leads to a pronounced intensity enhancement of the main lobe after propagating a certain distance. Concurrently, the width of the main lobe abruptly decreases, indicating that the beam is focusing on that point.

Several factors contribute to the observed enhancement ratio, with the most critical one being the parameter C. Detailed analysis reveals that increasing the absolute shift value C leads to an extended propagation distance as shown in Figure 4b, as the focusing consistently occurs when the main lobe intersects a trajectory aligned with the asymptote of the hyperbolic isofrequency contour. Under this condition, not only does the propagation distance increase, but a higher intensity enhancement ratio is also achieved as shown in Figure 4a. This is because more energy from the side lobes is gradually directed toward the main lobe during propagation, and the longer the beam travels, the more energy can be accumulated before focusing occurs.

In addition, increasing the magnitude of C leads to a broader initial intensity footprint, thereby necessitating a larger aperture to fully capture the spatial extent of the beam. Furthermore, material loss plays a crucial role in constraining the achievable enhancement ratio. As illustrated in Figure S2, there is a distinct loss threshold: below this threshold, the enhancement effect remains largely unaffected, but above it, the focusing behavior rapidly deteriorates. Notably, this threshold is not fixed—it varies with the value of C, highlighting the interplay between geometric parameters and material loss in determining the overall enhancement performance.

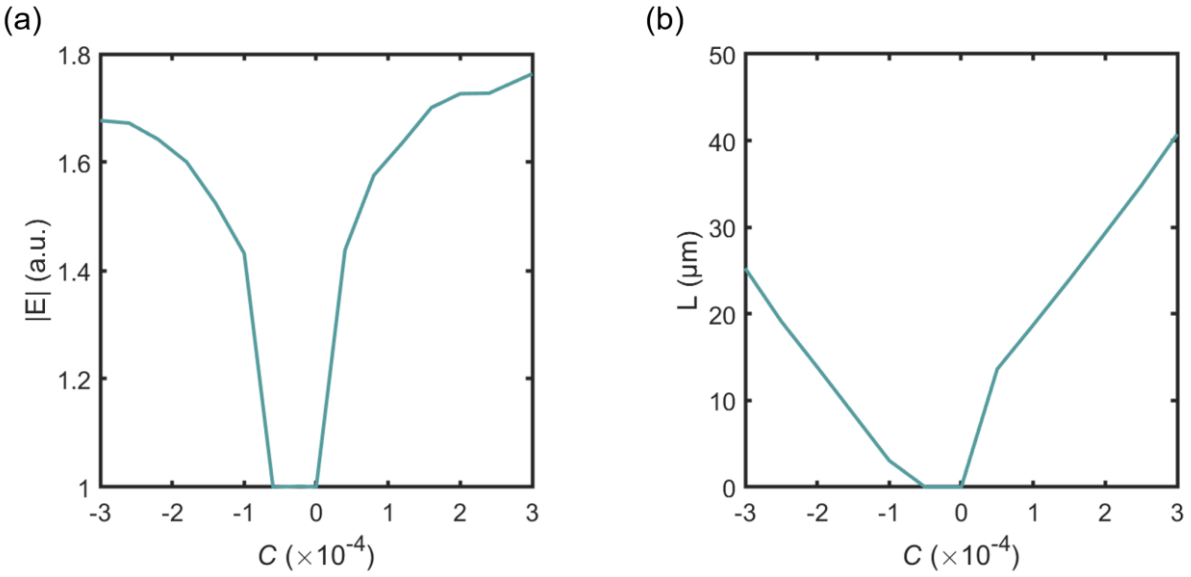


Figure 4. (a) The normalized electrical field for each shift value. The enhancement is positively correlated with the absolute value of parameter C. (b) The propagating length of the special beam, which increases linearly with the absolute shift value. Permittivity values are taken from α-MoO_3 at a frequency of $\omega = 910cm^{-1}$and order of $n = 40$.

Although the self-focusing effect can be achieved with both negative and positive shifts, there is a significant difference between them. Specifically, they exhibit entirely different behaviors along the asymptote direction. In the case of a negative shift value, the beam focuses only when the main lobe intersects the asymptote. This is evident from the intensity profile along the asymptote in Figure 5a, where a sudden increase in intensity occurs at the point of focusing. Conversely, for positive shift values, the intensity profile along the asymptote displays oscillations, corresponding to a multi-focusing process as shown in Figure 5b. Each time a side lobe intersects the asymptote, a focusing event occurs. As more side lobes become focused along the asymptote, the overall intensity gradually increases, eventually reaching a maximum when the main lobe is focused on the asymptote.

Recently, researchers have demonstrated an Airy-like special beam on the same in-plane hyperbolic α-MoO_3 platform[7], which shares certain similarities with our proposed self-focusing beam—most notably, both exhibit non-diffracting and self-bending propagation characteristics. However, we emphasize that these two beams are fundamentally different in terms of their underlying physical mechanisms.

Specifically, the Airy-like shear polariton is excited by an orbital angular momentum (OAM) beam that carries intrinsic angular momentum, which is not required in our design. This reflects their distinct physical origins: the Airy-like beam arises from the interaction between an OAM

excitation and hyperbolic media, whereas our beam is derived from a coordinate transformation of the isotropic Half-Bessel beam into the hyperbolic media. The difference is also evident in the beam propagation behavior. For the Airy-like shear polariton, switching between positive and negative OAM orders results in symmetric propagation patterns. In contrast, our beam shows an asymmetric response: positive and negative shift values lead to distinct self-focusing directions and intensity distributions.

In summary, while both the Airy-like shear polariton and our proposed self-focusing beam represent special beam solutions in hyperbolic media, they arise from fundamentally different physical origins and exhibit distinct propagation characteristics. Together, they highlight the diverse opportunities for advanced light manipulation enabled by extreme in-plane anisotropy in van der Waals materials.

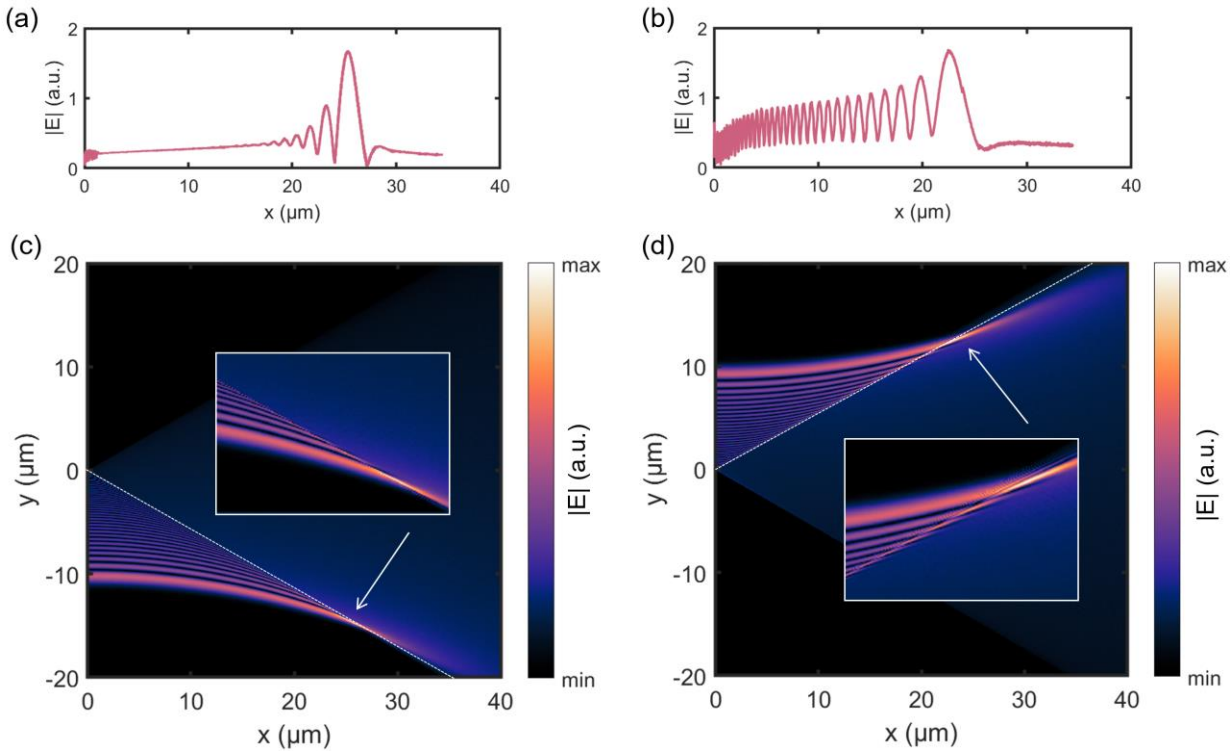


Figure 5. (a) The electrical field profile along the asymptote in (c) under $C = -16 \times 10^{-5}$. Intensity enhancement occurs only when the main lobe meets the asymptote. (b) The electrical field profile along the asymptote in (d) under $C = 28 \times 10^{-5}$. Intensity enhancement happens multi-times when each side lobe meets the asymptote. (c-d) The corresponding field distribution under positive and negative shift values, respectively, with zoomed-in figures illustrating the detailed light behavior along the asymptote. Permittivity is taken from α-MoO_3 at $\omega = 910 cm^{-1}$and $n = 40$.

5. Conclusion

In this study, we propose a novel design principle for constructing special beams in isotropic, elliptical, and hyperbolic media. Especially, the proposed scheme enables the creation of special beams in hyperbolic media that exhibit the unique self-focusing effect. By adjusting different shift values, the propagation length and intensity enhancement can be tuned with great flexibility, allowing for the realization of two distinct focusing mechanisms corresponding to negative and positive shift values, respectively. The proposed design principle can be extended to synthesize other kinds of special beams as well. Moreover, we demonstrate the design approach utilizing $A(\theta)$ of a Half Bessel beam in isotropic media can successfully realize the self-focusing effect. Notably, the application of our method is not limited to the specific cases discussed herein. By employing $A(\theta)$ to special beams, such as Airy beams, Mathieu beams, Weber beams, or any other type of special beam in isotropic media, they are all possible to be transformed into a corresponding special beam in elliptical or hyperbolic media using this method.

Funding:

National Research Foundation Singapore programme (NRF-CRP22-2019-0007, and NRF-CRP23-2019-0007); A*STAR grant numbers (M22K2c0080 and M23M2b0056); National Medical Research Council (NMRC) MOH-000927; the Distinguished Professor Fund of Jiangsu Province (Grant No. 1004-YQR24010); Fundamental Research Funds for the Central Universities, NUAA (No. NE2024007).

Disclosures:

The authors declare no conflicts of interest.

Yueqian Zhang and Haotian Wu contributed equally to this work.

References

[1] G. A. Siviloglou, J. Broky, A. Dogariu, D. N. Christodoulides, *Phys. Rev. Lett.* **2007**, *99*, 213901.
[2] I. Kaminer, R. Bekenstein, J. Nemirovsky, M. Segev, *Phys. Rev. Lett.* **2012**, *108*, 163901.
[3] P. Zhang, Y. Hu, T. Li, D. Cannan, X. Yin, R. Morandotti, Z. Chen, X. Zhang, *Phys. Rev. Lett.* **2012**, *109*, 193901.
[4] N. K. Efremidis, D. N. Christodoulides, **n.d.**
[5] I. Epstein, A. Arie, *Phys. Rev. Lett.* **2014**, *112*, 023903.
[6] J. Lin, J. Dellinger, P. Genevet, B. Cluzel, F. De Fornel, F. Capasso, *Phys. Rev. Lett.* **2012**, *109*, 093904.
[7] Y. Bai, Q. Zhang, T. Zhang, H. Lv, J. Yan, J. Wang, S. Fu, G. Hu, C. Qiu, Y. Yang, *Laser & Photonics Reviews* **2024**, *18*, 2400041.
[8] A. Salandrino, D. N. Christodoulides, **n.d.**
[9] P. Zhang, S. Wang, Y. Liu, X. Yin, C. Lu, Z. Chen, X. Zhang, *Opt. Lett.* **2011**, *36*, 3191.
[10] A. Minovich, A. E. Klein, N. Janunts, T. Pertsch, D. N. Neshev, Y. S. Kivshar, *Phys. Rev. Lett.* **2011**, *107*, 116802.
[11] A. E. Klein, A. Minovich, M. Steinert, N. Janunts, A. Tünnermann, D. N. Neshev, Y. S. Kivshar, T. Pertsch, *Opt. Lett.* **2012**, *37*, 3402.
[12] F. Bleckmann, A. Minovich, J. Frohnhaus, D. N. Neshev, S. Linden, *Opt. Lett.* **2013**, *38*, 1443.
[13] A. V. Singh, T. Pertsch, *Opt. Express* **2022**, *30*, 484.
[14] L. Li, T. Li, S. M. Wang, S. N. Zhu, *Phys. Rev. Lett.* **2013**, *110*, 046807.
[15] L. Li, T. Li, S. M. Wang, C. Zhang, S. N. Zhu, *Phys. Rev. Lett.* **2011**, *107*, 126804.
[16] S. S. Kou, G. Yuan, Q. Wang, L. Du, E. Balaur, D. Zhang, D. Tang, B. Abbey, X.-C. Yuan, J. Lin, *Light Sci Appl* **2016**, *5*, e16034.
[17] J. Lin, Q. Wang, G. Yuan, L. Du, S. S. Kou, X.-C. Yuan, *Sci Rep* **2015**, *5*, 10529.
[18] W. Pan, Z. Wang, Y. Chen, X. Zheng, S. Li, X. Tian, Q. He, L. Zhou, S. Sun, *ACS Photonics* **2023**, *10*, 2423.
[19] Y. Yang, H. T. Dai, B. F. Zhu, X. W. Sun, *IEEE Photonics J.* **2014**, *6*, 1.
[20] R. Li, M. Imran, X. Lin, H. Wang, Z. Xu, H. Chen, *Nanoscale* **2017**, *9*, 1449.
[21] Z. Liu, H. Lee, Y. Xiong, C. Sun, X. Zhang, *Science* **2007**, *315*, 1686.
[22] A. J. Hoffman, L. Alekseyev, S. S. Howard, K. J. Franz, D. Wasserman, V. A. Podolskiy, E. E. Narimanov, D. L. Sivco, C. Gmachl, *Nature Mater* **2007**, *6*, 946.
[23] C. R. Simovski, P. A. Belov, A. V. Atrashchenko, Y. S. Kivshar, *Advanced Materials* **2012**, *24*, 4229.
[24] A. A. High, R. C. Devlin, A. Dibos, M. Polking, D. S. Wild, J. Perczel, N. P. De Leon, M. D. Lukin, H. Park, *Nature* **2015**, *522*, 192.
[25] O. Y. Yermakov, A. I. Ovcharenko, M. Song, A. A. Bogdanov, I. V. Iorsh, Yu. S. Kivshar, *Phys. Rev. B* **2015**, *91*, 235423.
[26] W. Ma, P. Alonso-González, S. Li, A. Y. Nikitin, J. Yuan, J. Martín-Sánchez, J. Taboada-Gutiérrez, I. Amenabar, P. Li, S. Vélez, C. Tollan, Z. Dai, Y. Zhang, S. Sriram, K. Kalantar-Zadeh, S.-T. Lee, R. Hillenbrand, Q. Bao, *Nature* **2018**, *562*, 557.
[27] Z. Zheng, J. Chen, Y. Wang, X. Wang, X. Chen, P. Liu, J. Xu, W. Xie, H. Chen, S. Deng, N. Xu, *Advanced Materials* **2018**, *30*, 1705318.
[28] Z. Zheng, N. Xu, S. L. Oscurato, M. Tamagnone, F. Sun, Y. Jiang, Y. Ke, J. Chen, W. Huang, W. L. Wilson, A. Ambrosio, S. Deng, H. Chen, *Sci. Adv.* **2019**, *5*, eaav8690.
[29] G. Hu, A. Krasnok, Y. Mazor, C.-W. Qiu, A. Alù, *Nano Lett.* **2020**, *20*, 3217.
[30] G. Hu, Q. Ou, G. Si, Y. Wu, J. Wu, Z. Dai, A. Krasnok, Y. Mazor, Q. Zhang, Q. Bao, C.-W. Qiu, A. Alù, *Nature* **2020**, *582*, 209.

[31] M. Chen, X. Lin, T. H. Dinh, Z. Zheng, J. Shen, Q. Ma, H. Chen, P. Jarillo-Herrero, S. Dai, *Nat. Mater.* **2020**, *19*, 1307.
[32] G. Hu, C.-W. Qiu, A. Alù, *Opt. Mater. Express* **2021**, *11*, 1377.
[33] H. Hu, X. Lin, G. Hu, F. J. Garcia-Vidal, Y. Luo, *InfoScience* **2024**, e12024.
[34] Q. Zhang, Q. Ou, G. Hu, J. Liu, Z. Dai, M. S. Fuhrer, Q. Bao, C.-W. Qiu, *Nano Lett.* **2021**, *21*, 3112.
[35] J. Duan, G. Álvarez-Pérez, K. V. Voronin, I. Prieto, J. Taboada-Gutiérrez, V. S. Volkov, J. Martín-Sánchez, A. Y. Nikitin, P. Alonso-González, *Sci. Adv.* **2021**, *7*, eabf2690.
[36] Y. Zeng, Q. Ou, L. Liu, C. Zheng, Z. Wang, Y. Gong, X. Liang, Y. Zhang, G. Hu, Z. Yang, C.-W. Qiu, Q. Bao, H. Chen, Z. Dai, *Nano Lett.* **2022**, *22*, 4260.
[37] N. A. Aghamiri, G. Hu, A. Fali, Z. Zhang, J. Li, S. Balendhran, S. Walia, S. Sriram, J. H. Edgar, S. Ramanathan, A. Alù, Y. Abate, *Nat Commun* **2022**, *13*, 4511.
[38] G. Lu, Z. Pan, C. R. Gubbin, R. A. Kowalski, S. De Liberato, D. Li, J. D. Caldwell, *Advanced Materials* **2023**, *35*, 2300301.
[39] Z. Dai, G. Hu, G. Si, Q. Ou, Q. Zhang, S. Balendhran, F. Rahman, B. Y. Zhang, J. Z. Ou, G. Li, A. Alù, C.-W. Qiu, Q. Bao, *Nat Commun* **2020**, *11*, 6086.
[40] Y. Wu, Q. Ou, Y. Yin, Y. Li, W. Ma, W. Yu, G. Liu, X. Cui, X. Bao, J. Duan, G. Álvarez-Pérez, Z. Dai, B. Shabbir, N. Medhekar, X. Li, C.-M. Li, P. Alonso-González, Q. Bao, *Nat Commun* **2020**, *11*, 2646.
[41] Y. Wu, Q. Ou, S. Dong, G. Hu, G. Si, Z. Dai, C. Qiu, M. S. Fuhrer, S. Mokkapati, Q. Bao, *Advanced Materials* **2021**, *33*, 2008070.
[42] H. Hu, N. Chen, H. Teng, R. Yu, Y. Qu, J. Sun, M. Xue, D. Hu, B. Wu, C. Li, J. Chen, M. Liu, Z. Sun, Y. Liu, P. Li, S. Fan, F. J. García De Abajo, Q. Dai, *Nat. Nanotechnol.* **2022**, *17*, 940.
[43] Q. Zhang, Q. Ou, G. Si, G. Hu, S. Dong, Y. Chen, J. Ni, C. Zhao, M. S. Fuhrer, Y. Yang, A. Alù, R. Hillenbrand, C.-W. Qiu, *Sci. Adv.* **2022**, *8*, eabn9774.
[44] H. Hu, N. Chen, H. Teng, R. Yu, M. Xue, K. Chen, Y. Xiao, Y. Qu, D. Hu, J. Chen, Z. Sun, P. Li, F. J. G. De Abajo, Q. Dai, *Science* **2023**, *379*, 558.
[45] H. Teng, N. Chen, H. Hu, F. J. García De Abajo, Q. Dai, *Nat Commun* **2024**, *15*, 4463.
[46] K. Wang, Z. Huang, L. Xiong, K. Wang, Y. Bai, H. Long, N. Deng, B. Wang, G. Hu, P. Lu, *Optica* **2025**, *12*, 343.
[47] Q. Zhang, G. Hu, W. Ma, P. Li, A. Krasnok, R. Hillenbrand, A. Alù, C.-W. Qiu, *Nature* **2021**, *597*, 187.
[48] D. Lee, S. So, G. Hu, M. Kim, T. Badloe, H. Cho, J. Kim, H. Kim, C.-W. Qiu, J. Rho, *eLight* **2022**, *2*, 1.
[49] G. Álvarez-Pérez, T. G. Folland, I. Errea, J. Taboada-Gutiérrez, J. Duan, J. Martín-Sánchez, A. I. F. Tresguerres-Mata, J. R. Matson, A. Bylinkin, M. He, W. Ma, Q. Bao, J. I. Martín, J. D. Caldwell, A. Y. Nikitin, P. Alonso-González, *Advanced Materials* **2020**, *32*, 1908176.
[50] G. Álvarez-Pérez, K. V. Voronin, V. S. Volkov, P. Alonso-González, A. Y. Nikitin, *Phys. Rev. B* **2019**, *100*, 235408.